ISSN (e): **2250 – 3005** || *Volume, 07* || *Issue, 11*|| *November – 2017* ||
International Journal of Computational Engineering Research (IJCER)

Precise assembly and joining of silver nanowires in three dimensions forhighly conductive composite structures

[1]nidhi Khobragade, [2]sonismita Moharana
Gandhi Institute of Excellent Technocrats, Bhubaneswar, India
Black Diamond College of Engineering & Technology, Jharsuguda, Odisha, India

ABSTRACT:
Three-dimensional(3D)electricallyconductivemicro/nanostructuresarenowakeycomponentinabroad range of research and industry fields. In this work, a novel method is developed to realize metallic3Dmicro/nanostructureswithsilver-thiol-acrylatecompositesviatwo-photonpolymerization followedbyfemtosecondlasernanojoining.Complex3Dmicro/nanoscaleconductivestructureshavebeensuccessfullyfabricatedwith~200nmresolution.Theloadingofsilvernanowires(AgNWs)andjoining of junctions successfully enhance the electrical conductivity of the composites from insulating to92.9Sm^{-1}atroomtemperature.Moreover,forthefirsttime,areversibleswitchingtoahigher conductivityisobserved,upto~ $10^5 Sm^{-1}$at523K.Thetemperature-dependentconductivityof the composite is analyzed following the variable range hopping and thermal activation models.
The nanomaterial assembly and joining method demonstrated in this study pave a way towards a wide range of device applications, including 3D electronics, sensors, memristors, micro/nanoelectromechanicalsystems, and biomedical devices, etc.
Supplementary material for this article is available online
Keywords: precise assembly, joining, silver nanowires, nanofabrication, three dimensional

I. INTRODUCTION

Over the last decade, micro/nanostructures have been receiving increasing attention due to their potential applications in modern
nanotechnology andemerging fields, such as microelectronics
[1], flexible electrodes [2], micro/nanoelectromechanicalsys- tems(MEMS/NEMS) [3], photonics and optoelectronics[4],
metamaterials [5], and energy storage [6]. As it becomes increasingly challenging for Moore's Law to continue to push the two-dimensional miniaturization limit toward the atomic level, research on the integration/assembly of functionalmicro/
nanostructuresin three-dimensional (3D) space fordevice
applicationsis becoming increasingly important [7]. Direct laser writing by two-photon polymerization (TPP) has been estab- lishedasoneofthemostpromisingmethodsforachieving3D
fabricationin micro/nanoscales, due to its ability to produce arbitrary and complex 3D structures with subwavelengthreso- lution[8]. However, the lack of TPP-compatible and functional materials represents a significant barrier to realize the function- alityof the fabricated devices, such as high electrical con- ductivity, high environmental sensitivity, high mechanical strength, etc[9].
Recently, several studies have demonstrated the use of TPP for the fabrication of electrical conductive micro-structures, including selective plating [10], metallic inversion [4],insituphotoreductionwithphotopolymerization[11],and direct photopolymerization of composite resins [12]. Both selective plating and metallic inversion methods involve multiple, time- and cost-intensive synthetic steps. In situ photoreduction synthesis allows single-step fabrication of two-dimensional patterns of noble metallic NPs [11], discrete NP-dopedpolymermicrostructures[11],andevenbridge-like conductive elements [11]. However, this method is intrinsi- cally difficult to simultaneously satisfy precise morphology andhighelectricalconductivity[13].Inourpreviouswork,
multiwalled carbon nanotubes (MWNTs) were employedfor
thefabricationof3Dconductivemicro/nanostructures[12].

The composite photoresist showed significantly enhanced electricalconductivity(upto46.8Sm^{-1}@0.2wt%MWNTs), with strong anisotropic properties and highoptical transmittance. Nevertheless, the composite conductivity is stilllimitedbytheintrinsicconductivityofMWNTs(roughly $5\times10^{3}$to$5\times10^{6}Sm^{-1}$)[14]andrelativelyhightube-to-tube contact resistance. Compared with carbon nanotubes, silver(Ag)isconsideredtobeanidealconductivematerial ($6.3\times10^{7}Sm^{-1}$).Thesmalldimensionandhighaspectratio ofone-dimensionalsilvernanowires(AgNWs)couldeffec- tively transport electrical carriers along one controllable path [15],andmoreover,interconnectednanowirenetworkscan be realized by the wire-to-wire junction joining/welding [2, 16], thereby leading to increased electrical properties with a low nanofiller loading concentration. However, to the best of our knowledge, 3D AgNWs-based micro/nanostructures of high electrical conductivity and surface morphology have notbeen realizedyet.

In this paper, we report a method for designing and pre- paring a TPP-compatible AgNW-thiol-acrylate (ATA) composite photoresist andsimultaneously achieving reliable 3D micro/ nanofabricationwithhighstructuringaccuracyandhighelectrical conductivity (figure 1(a)). Moreover, afemtosecond laserwas usedfor the nanojoiningof AgNW junctions inside a polymer matrix to further reduce the wire-to-wire junction resistance and thus increase the electric conductance of the overall 3D micro/ nanostructure substantially. Finally, the temperature-dependent electricalconductivityandtheresistanceswitchingmechanismof the as-fabricated ATA bridge structures were investigatedby employingthe variable range hopping (VRH) model andthermal activationestimation.Theas-fabricatedbridgestructuresmadeof ATA composites showed a substantial three-step increase in electrical conductivity over ten-orders of magnitude with the AgNWaddition, femtosecond laser nanojoiningandresistive switching, respectively (figure 1(b)). Thesenanocomposites aredistinctfromtheconventionalviewoftheelectricalproperties inpolymer nanocompositesas either insulating or conducting below and above the percolation threshold, respectively. The fabrication method simultaneously realized the user-defined arbitrary 3D micro/nanostructuring, high spatial resolution, fine surfacequality,andsuperiorelectricalconductivity,whichmakes it promising for various functional device applications, including 3Delectronics,sensors,plasmonics,memristors,MEMS/NEMS, and biomedical devices, etc.

II. RESULT AND DISCUSSION

Preparation of ATA compositeresin

TheTPP-compatibleATAcompositeresinswerepreparedby directly mixingthiolatedAgNWs with acrylate-based resin (table S1, supporting information available online at stacks.iop.org/IJEM/1/025001/mmedia) and characterized using transmissionelectronmicroscopy(TEM)andmassspectro- metry. Silver nanowires were used in the composites with lengths ranging from 0.1 to 4.15 μm and concentrationsfrom 0.005 to 0.4 wt%. Nanowires with an average diameter of 40 nm and lengths from 0.48 to 4.15 μm were prepared by breaking >30 μm long AgNWs using ultrasonicvibration (figuresS1(a)–(e),supportinginformation).UsingTPPpro- cessingtofabricatestructures,thelaserbeamwillbescattered by agglomerated nanowires at high concentration, which will distort the fabricated structures. Therefore, themaximum 0.4 wt% AgNW concentration was chosen to avoid agglom- eration until changes in the electrical properties of the com- posites reaching a plateau value. Moreover, it is expectedthat shorterAgNWscouldresultinbetterdispersionandsmoother composite structure surfaces compared with longer ones. However, a balance on AgNW length should be considered since it is easier to form a connecting network in polymers with the same effective concentration by using longer AgNWs. To obtain stable and homogeneous dispersion of AgNWs, thiolwith a suitable length of carbon chains ($HOC_nH_{2n+1}SH$, n = 6) was used as the surfactant in the composite resins (figure 2(a)). The composite resinsappeared to be stable under ambient conditions with a color transition from clear to gray as the AgNW concentrationincreased (figure 2(b)).

TEM images of the ATA composite (figure 2(d))were capturedbydirectlyanalyzingthethinfilmmadebyTPPwith a thickness of ~1 μm on a copper grid. A shell (2–4 nm thickness)comprisedofmultiple,intertwinedlayersofthiol molecules formed on the surface of the AgNWs, as the

thiolsulfurformedastrongchemicalbondwithAg[17],leaving theothergroup(OH)miscibleintheacrylateresintoundergo subsequentpolymerizationreactions[18](magnifiedimagein figure2(d),figuresS1(f)and(g),supportinginformation). The thiol layer allowed the individual AgNWs to maintain distance between each other, preventing them from aggrega- tion and causing the resulting thiolatedAgNWs to be well dispersedinthepolymermatrix.InadditiontoTEMchar- acterization, a KrFexcimer laser (248 nm, 23 ns) was usedto assistlaserablationinambientmassspectrometryusinga

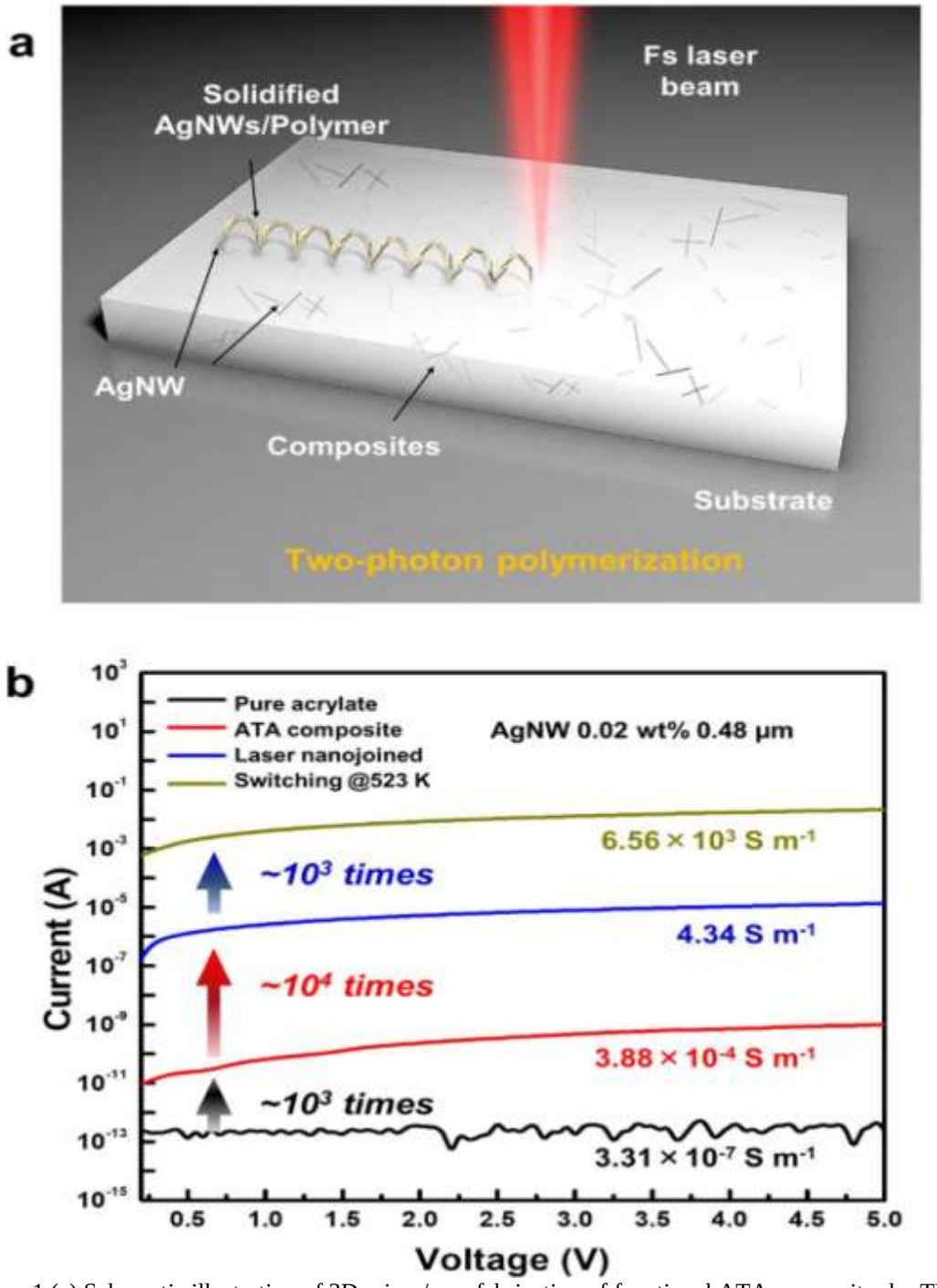

Figure 1.(a) Schematic illustration of 3D micro/nanofabrication of functional ATA composites by TPP lithography. (b) I–V curves of bar- shaped channels fabricated using pure acrylate (black) and ATA composite (red), after laser nanojoining (blue), and thermally treated at 523K(yellow).TheAgNWconcentrationandlengthwere0.02wt%and0.48μm,respectively.

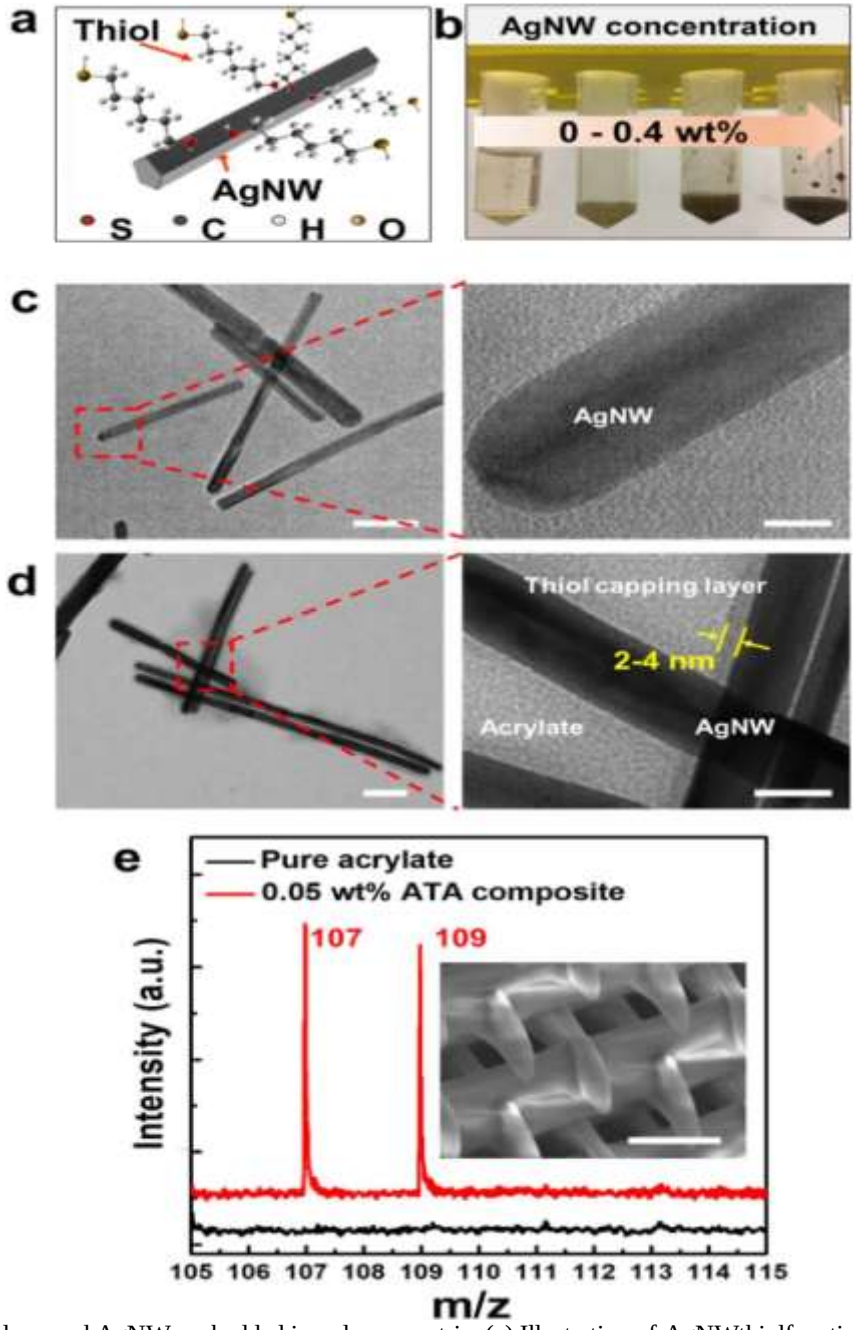

Figure 2.Thiol-capped AgNWsembedded in polymer matrix. (a) Illustration of AgNWthiolfunctionalization. (b) Optical image of the ATA composite resins with 0, 0.05, 0.2, and 0.4 wt% AgNWconcentrations. The AgNWlength was kept at 0.48 μm. TEM micrographs of (c) AgNWs and (d) thiol-capped ATA composite thin film. (e) Mass spectra of micro-woodpile structures fabricated using pure acrylate and the ATA composite. Inset shows the SEM micrograph of the woodpile fabricated using the composite resin (0.05 wt% AgNWconcentration, 0.48 μmAgNWlength).
Thelaserpowerandscanningspeedwere17.5mWand50μms^{-1},respectively.Scalebar:(c),(d)left100nm,right10nm;(c)inset 2μm.

time-of-flight mass spectrometer (TOF-MS). Two prominent peaks were observed in the spectra of a micro-woodpile compositestructure,at107and109,whichwereascribedto isotopes of ^{107}Ag and ^{109}Ag, respectively (figure 2(e))[19].A clearchangeincontrastwasobservedinthescanningelectron microscopy (SEM) image of the micro-woodpile (figure 2(e) inset),indicatingacompositionaldifferenceofmetallicphase inside the polymer matrix, revealing the existence of the AgNWs in the ATA composite [20]. The SEM and TEM resultsprovideexperimentalevidencethattheAgNWswithin

thepolymermatrixdistributedinacombinedwayofseparate nanowires and connected networks. Therefore, TPP-compa- tibleATA composite resins, with thiolatedAgNWs uniformly dispersed in the acrylate resins, were successfully prepared. Our approach also paves a way for dispersion and assembly of various functional nanomaterialsinto 3D polymer structures, including carbon nanotubes, metallic NPs, semiconductor NPs or magnetic NPs, for the fabrication of advanced micro/nano- devices with additional functionalproperties.

Fabrication of 3D metallicmicro/nanostructures

After identification and characterization of the composite resins, the ATA composites were employed to fabricate conductive 3D micro/nanostructures with high spatial reso- lution and fine surface quality. An integrated set ofbeam transport optics directed the laser output with circular polar- ization to a final focusing objective (63×, NA = 1.4) that scanned in 3D according to the user-defined geometric designs and assemble AgNWs within the focal spot. After TPP lithography, the samples were developed. The unsolidi- fied resin was rinsed away, leaving AgNWs embeddedinside thesolidifiedATAcompositestructuresonthesubstrates.

Figures3(a)–(h)showsexamplesof3Dmicrostructuresmade from the ATA composite resins with various AgNW lengths on both rigid and flexible substrates. A spiral-like photonic crystal and large-scale gratings were fabricated with 0.48μm longAgNWs embedded and confined within the composite lines (figures 3(a)–(d)). A suspended microbar, arc-shaped wire bonding bridges, a microhelix, and a microcapacitor were fabricated using ATA composite with 0.1 μmlong AgNWs (figures 3(e)–(h)). The TPP fabrication was inde- pendent of substrates, which can be conducted on either flexible polyethylene terephthalate (PET) or rigid substrates, such as silicon (Si) wafer and glass substrates.

To optimize the laser fabrication condition, the depend- ence of structural resolution on the laser power (figure 3(i)) was carefully evaluated. Large parallel cuboid supportswere fabricated first, and then a series of lines were scannedacross thesupports.Thesuspendedlineswerefabricatedusingdif- ferent laser powers and a fixed writing velocity of $100\mu ms^{-1}$.Aminimumlinewidthof202±18nmwasobservedatapolymerizationthresholdpowerof3mW.It wasalsofoundthatthefeaturesizeofthefabricatedwoodpile structures decreased with the existence of AgNWs inthe compositeunderthesameprocessingconditions(figureS2, supporting information). The line width of the sample pre- pared with 0.2 wt% AgNWs exhibited a ∼15% decrease compared with that of pure acrylate structure, which can be attributed to absorption by AgNWs in the path of the laser beam prior to reaching the focal point [21].

The elliptically shaped cross-section was revealed by multi-photon ablation (MPA) on the solidified grating struc- tures on a glass substrate (figure S3, supporting information). This ‘TPP + MPA’ method has been demonstrated to be an effective technique for the fabrication of microvoidsand microfluidicstructures[22].Polarizationofthelaserbeamhas been reported to affect the intensity distribution and thermal gradients around the focal spot thus leading to different polymerization rates, which can, in certain cases, affect the feature size [23]. In our work, the circular polarization of incident light could ensure a more spherical voxel within the xy-plane [24] and avoid polarization-dependentlinewidth.

The electrical conductivity of the composites was char- acterized by performing cyclic I–V measurements of 100 μmlonglineandbar-shapedchannelbridgingtwopairsofgold (Au) electrodes. A single line was fabricated using the ATA composite (0.05 wt% AgNW concentration, 0.1 μmlong- AgNWs), and the resulting conductivity from I–V measure- mentwascalculatedtobe$12.5Sm^{-1}$(figureS3(c),sup-porting information). Bar shape channels with across-section of$5\times5\mu m^2$werefabricatedinthefollowingexperiments, due to the multilayer structure of the host polymer could provide sufficient charge carriers’ transport channels (i.e. connected AgNWjunctions in 3D), and therefore avoid instability compared with single layer or line structures. Figure 3(j) shows the electrical conductivity of theATA composites as a function of AgNW concentrations at a fixed AgNW length of 0.1 μm. The experimental results indicate thattheAgNWloadingplaysasignificantroleindetermining the conductivity of the composites. With only 0.005 wt% AgNWsloadedintotheacrylateresin,anapproximateseven- orders of magnitude increase in the electrical conductivity was observed, which could be ascribed to the highly uniform distribution of short-length AgNWs. The conductivity of the composite polymers increased as the AgNWconcentration

increasedandreachedamaximumof32.51Sm^{-1}at0.2wt%
AgNW concentration. Furthermore, the effect of AgNWlengthonconductivityisshowninfigure3(k).Withafixed
0.02wt%AgNWconcentration,theconductivityincreased
from2.35×10^{-4}to1.13×$10^{-3}$$Sm^{-1}$astheAgNWlengthincreasedfrom0.3to1.35µm,duetothereduced
nanowire distance and sufficient conduction pathways estab- lished by the longer AgNWs. However, as the AgNW length exceeded 1.35 µm, the conductivity of the ATA composite dropped slightly. The 4.15 µm long AgNWs were prone to forming larger aggregates which were centrifuged out of the composite resin, thus the ATA composite would have a smaller'effective'fillerconcentration.Thesamephenomenon was observed for the composite with 0.1 µm long AgNWsat
a 0.4 wt% loading concentration (figure 3(j)). Moreover,long
AgNWs tended to produce a high number of networked AgNWs with a relatively large nanowire cross-junction resistance [25]. Consequently, the as-fabricated conductivity
oftheATAcompositeswith0.3–4.15µmlongAgNWs($10^{-4}$to$10^{-3}$$Sm^{-1}$)waslowerthan0.1µmlongAgNWsatthe

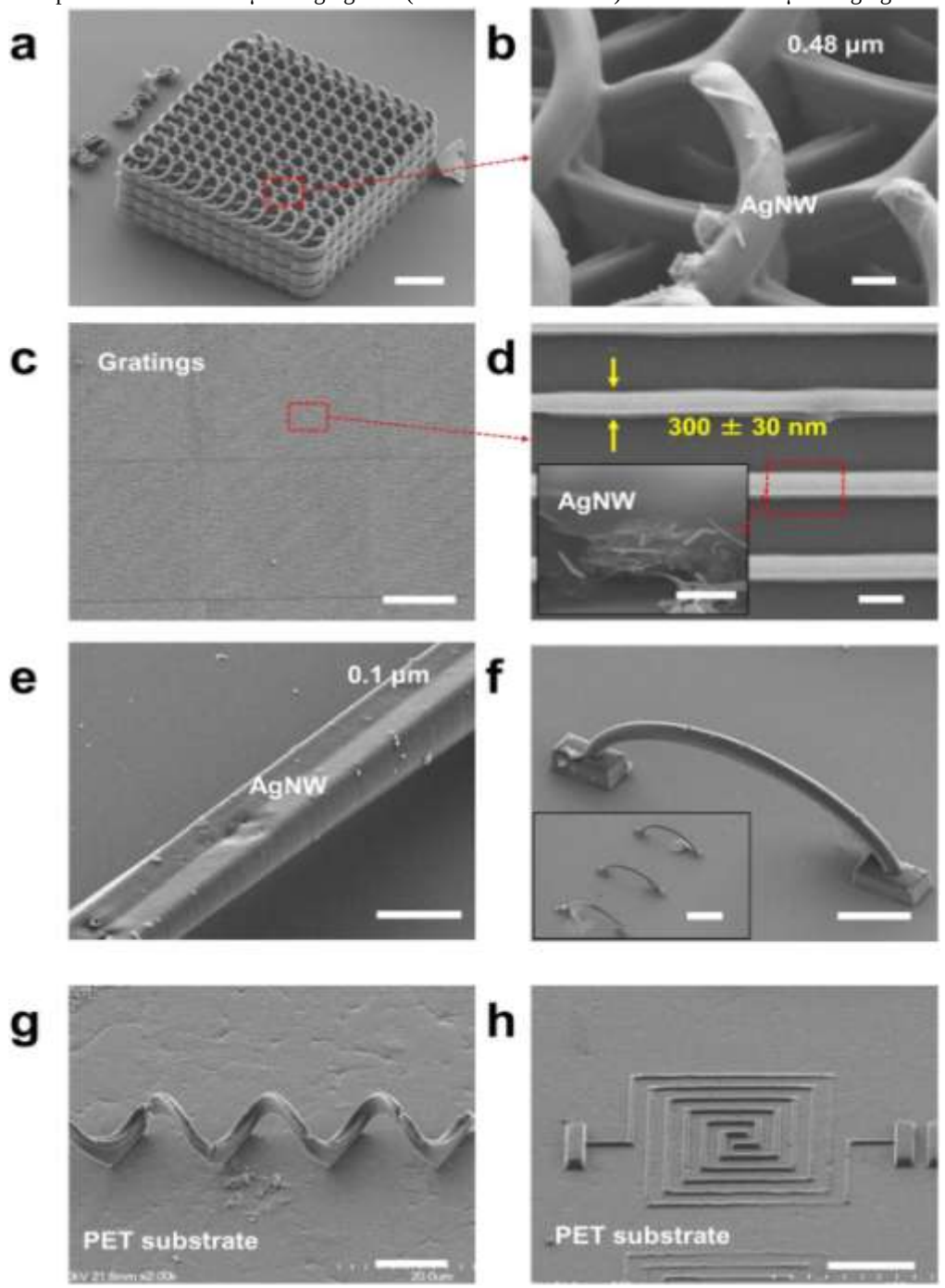

Figure 3.SEM micrographs of various functional micro/nanostructures fabricated on (a)–(f) rigid Si/SiO_2 substrates and (g), (h) flexible PET substrates, including (a), (b) a spiral-like photonic crystal, (c), (d) large-scale gratings, (e) a suspended microbar, (f) arc-shaped wire bonding bridges, (g) a microhelix, and (h) a microcapacitor. The AgNW length was 0.48 μm for (a)–(d) and 0.1 μm for (e)–(h). The laser powerandscanningspeedusedintheTPPfabricationwere(a),(b),(g)12.5mWand25μms^{-1},(c)–(e),(h)25mWand1mms^{-1},and (f)17mWand1mms^{-1},respectively.AthinlayerofNiwascoatedonthebackoftransparentPETsubstratetogeneratesuffici entrefractive index difference with the composite resin. (i) Dependence of feature size on the laser power used for TPP lithography. The inset is a suspended line with a minimum line width of 202 ± 18 nm fabricated using the ATA composite resin with a 0.2 wt% AgNW concentration and a 0.1 μmAgNW length. (j) Electrical conductivity of the ATA composites with respect to the AgNW concentration. The AgNW length was kept at 0.1 μm. The inset shows the SEM micrograph of a microbar-shaped channel. (k) Electrical conductivity of the ATA composites with respect to the AgNW length. The AgNW concentration was kept at 0.02 wt%. Scale bar: (a) 10 μm; (b) 1 μm; (c) 50 μm; (d) 500 nm; (e) 5 μm; (f) 20 μm, inset: 50 μm; (g) 10 μm; (h) 50 μm; (j) inset: 20 μm.

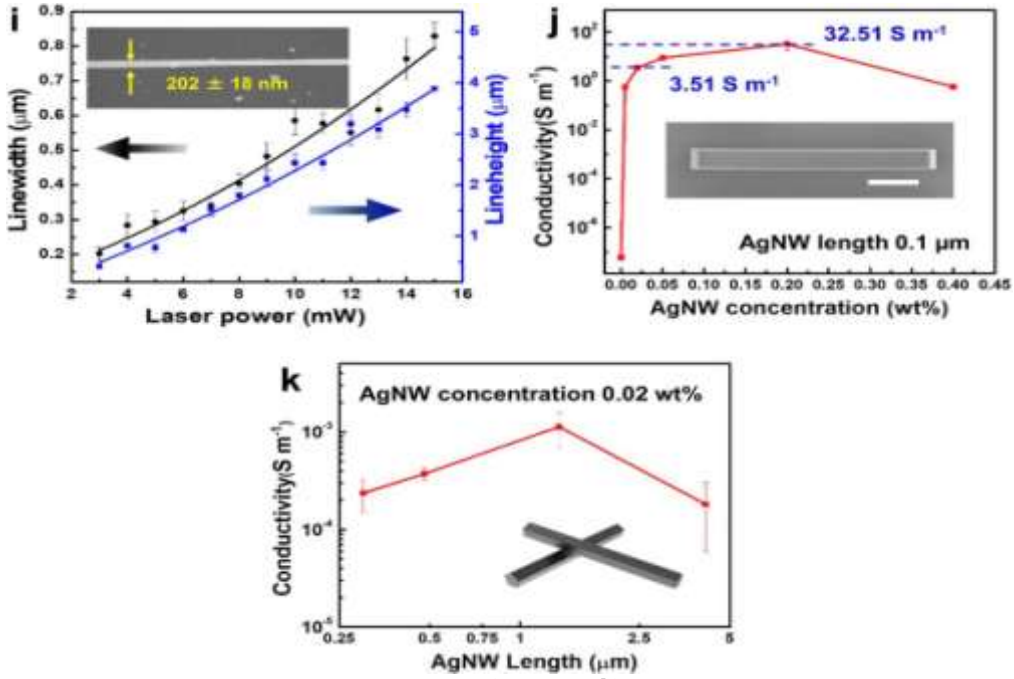

Figure 3.(Continued.)

sameconcentration(3.51Sm^{-1},figure3(j)).BasedontheATA composites, the TPP technique offered arbitrary 3D structuringcapabilitywithrelativelyhighelectricalconductivityaswellassubmicronspatialresolution.However,in the ATA composites, although the thiol sheath layer sig- nificantly enhanced the disperse quality of the AgNWs in the polymer matrix, it also introduced conduction barriers between nanowires. Therefore, the authors needed to find a way to further enhance the electrical conductivity of the as- fabricated 3Dmicro/nanostructures.

Laser joining of the AgNWjunction

With an aim of optimizing the electrical conductivity of the ATA composites, a nanojoining process was developedusing femtosecond laser pulses to further reduce the wire-to-wire junction resistance of AgNWs. A variety of attempts have been made to improve the junction contacts, including Joule heating [26], thermal annealing [27], mechanical pressing [28], and plasmonic welding [29]. However, the highsurface- to-volume ratio of the AgNWs makes them vulnerable to traditional thermal treatments which cause the AgNWsto undergo a morphological instability and fragmentation intoa chain of nanospheres, due to the Rayleigh instability (figure S4, supporting information) [30]. This instability presented a challenge to applying thermal annealing as a method of reducing the junction resistance of AgNWs.Femtosecond laser-inducedplasmonic joining appeared to be a good can- didate in terms of noncontact processing and

minimum thermal damage to the nanowires and the substrate [29]. It is known that femtosecond laser irradiation can deposit energy with a time scale shorter than the electron–phonon equili- brium time and constrain the heat generation within a well- definedhotspotregiondeterminedbythedistributionofthe localized electrical field between the gap of AgNWs[29, 31].AfterTPPfabrication,afemtosecondlaser(1kHzamplifiedTi:sapphirelasersystem,LegendF,CoherentInc.)at800nm wasused to join the junctions of AgNWs inside the composite structures (figure 4(a)). As shown in figure 4(b), thenanojoining process can be described in three stages: (1) high intensitylaser field was concentrated at the AgNWjunctions, which initiated thedecompositionofthethiollayerandsoftenedthelatticeof theAgNWs [32]; (2) the Ag atoms at the junctionwere ther- mally excited, and some portion of the material was ejected in the form of NPs (supported by the formation of NPs after laser irradiation, figure S5, supporting information); and (3)these excitedNPs possessed high mobility, which diffused to the AgNWjunctionsandenabledtheAgNWstobejoinedlocally (figure 4(d), figure S6, supporting information).

Inafirstattempt,AgNWnetworkswereirradiatedwith differentlaserenergiestoobtainoptimizedparameters(figure S6,supportinginformation).Asthenetworkwasprocessed withasufficientlaserfluence(35mJcm^{-2}),theSEMimages showedevidenceofspheroidization,fusion,andsignificant

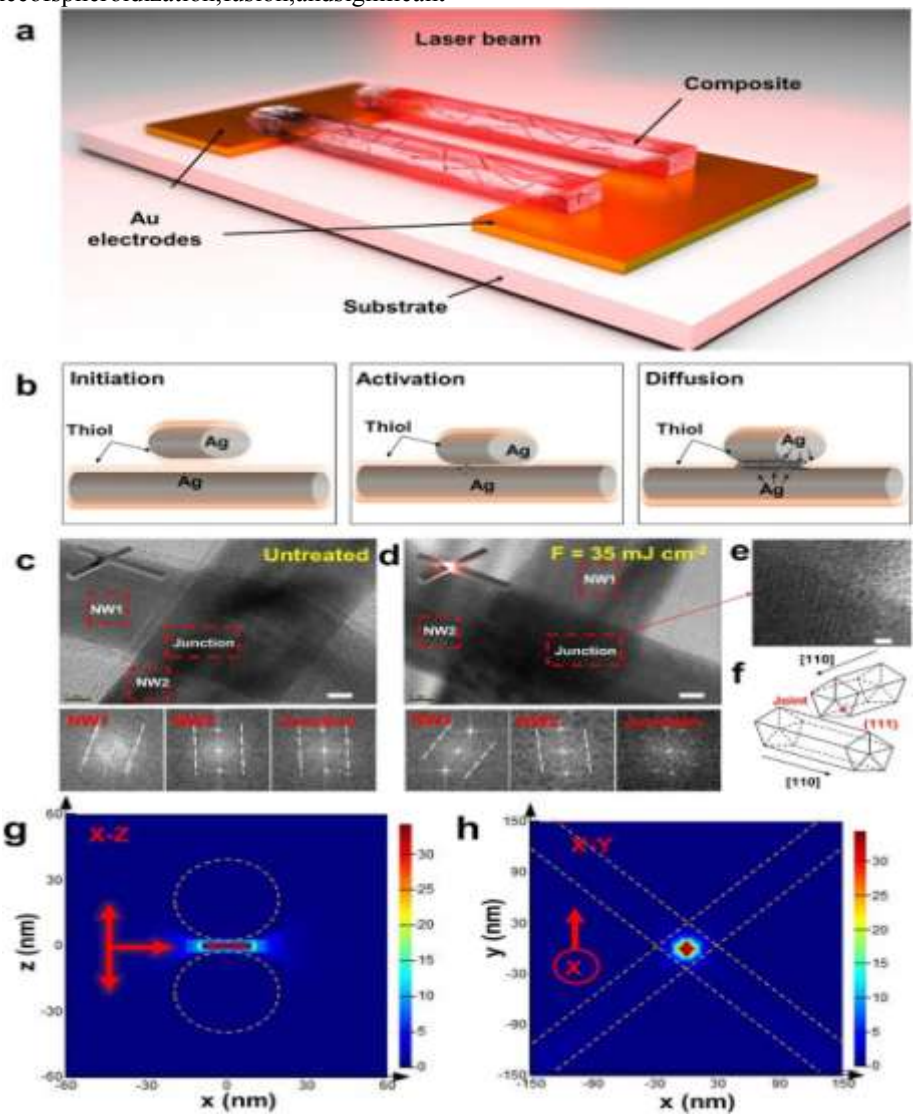

Figure 4.Femtosecond laser nanojoining of AgNW junctions within the ATA composites. (a) Schematic of the laser nanojoining process. (b)Illustrationofjoiningprocessrepresentedbycross-sectionalviewsoftheAgNWjunctions(i)initiation,(ii)activation,and(iii)diffusion. TEMmicrographsofAgNWjunctionswithinthecompositethinfilm(c)beforeand(d)afterlaserirradiation.Insetsrepres enttheFFT patterns of selected areas of NW 1, NW 2, and junction. Parallel lines in the insets show the crystal orientations

in different areas.
(e) Magnified HRTEM image of the joint area formed by laser nanojoining. (f) Scheme of AgNW joining by merging over (111) growing plane, where central axis of the AgNWs in the [110] direction. (g), (h) FDTD simulation of irradiance intensity distributions at the AgNW junction in XZ and XY planes. Dashed circles and lines indicate the AgNWs with the diameter of 40 nm and the length of 0.48 µm. The gap
distance was set to be 4 nm in the z direction. The electric field of the incident beam was in the YZ-plane (double arrow), and incident radiationpropagatedintheydirection(singlearrow).(i)I–Vcurvesofabar-shapedchannelbeforeandafterfemtosecondlasernanojoining. The AgNW concentration and length were 0.02 wt% and 0.48 µm, respectively. (j) Electrical conductivity of the ATA composites before (blackcurve)andafterlasernanojoining(redcurve)withrespecttotheAgNWconcentration.TheAgNWlengthwaskepta t0.1µm.
(k) Electrical conductivity of the ATA composites before (black curve) and after laser nanojoining (red curve) with respect to the AgNW length. The AgNW concentration was kept at 0.02 wt%. Scale bar: (b) inset: 50 µm; (c), (d) 5 nm; (e) 1 nm.

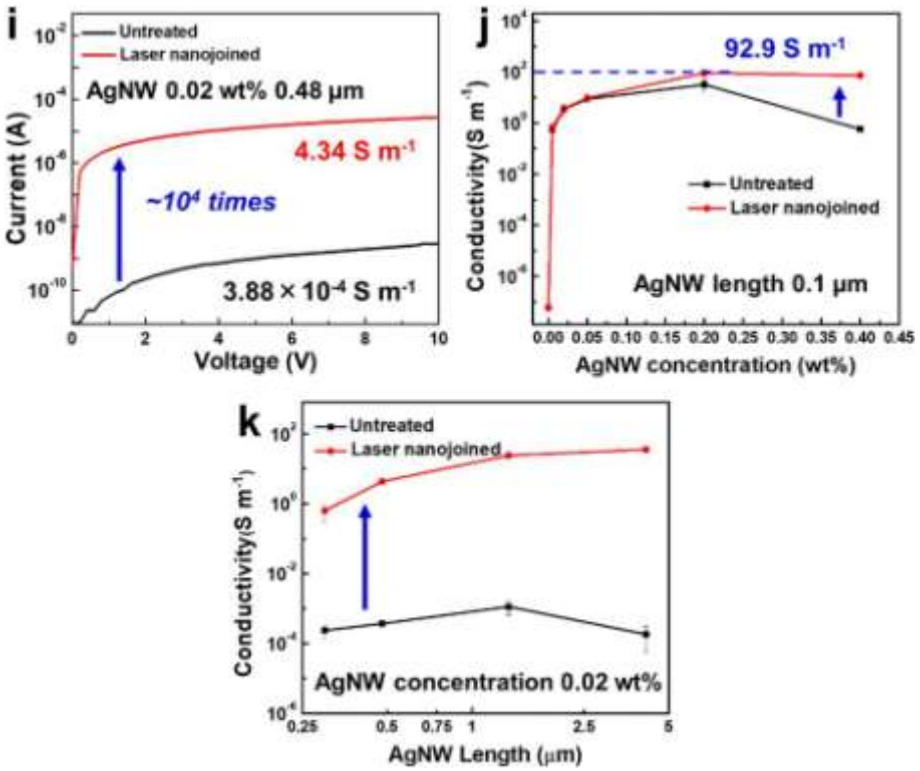

Figure 4.(Continued.)

local change in morphology at the junctions, while the rest of the AgNWs remained intact. A further increase in laser flu- ence induced photofragmentation and caused the breakup of the AgNWs [33]. Once the optimized irradiation conditions were obtained, laser nanojoining was carried out on the solidifiedATAcompositesaftertheTPPprocess.TheATA
compositefilmswerehighlytransparentat800nm(figureS7, supporting information), thus enabling laser energy tobe
predominately absorbed by the AgNWs for proper nano- joining. High resolution TEM (HRTEM) images of the AgNW junctions before and after laser irradiation areshown
in figures 4(c) and (d). Fourier spectra were obtained by fast- Fourier transform (FFT) from three different areas in each
figure.Beforelaserirradiation,twoAgNWswerelaidoneach other and separated by the thiol sheath. The diffraction pat- terns of the two nanowires were visible along two different directions,withroughlyequalintensityandcertainrotation
symmetry (~45°). These diffraction patterns represented the
[110] growth direction of the AgNWs (the long axis of the nanowires). The junction showed diffraction spots primarily
alongasingledirection,matchingthediffractionpatternfrom the bottom nanowire. After laser illumination, the

diffraction patternsandlatticestructuresatthecontactjunctionwere
different from both of the individual nanowires (figures 4(d) and (e)). This revealed a localized laser-induced Ag atom diffusionandrecrystallizationfollowingthe(111)planeatthe junction area during laser irradiation [34] (figure4(f)).
Moreover, it is important to point out that the original crystal orientation was intact in each NW at locations away from the junction.
A four-orders of magnitude increase in electrical con- ductivity,from~3.88×10^{-4}to4.34Sm^{-1},wasobservedina bar-shaped channel structure fabricated using the ATA composite (0.02 wt% AgNW concentration, 0.48 μmlong-
AgNWs) after laser illumination, indicating thesuccessful
nanojoining of AgNWs inside the composites (figure 4(i)). In
addition, the laser nanojoining process was demonstrated to be more effective on composite resins with longerAgNWs
(figures4(j)and(k)).Theenhancedelectricalperformance
was gauged by the ratio of the conductivity with and without laser irradiation ($\sigma_{joined}/\sigma_{as\text{-}fabricated}$). For the ATA composite with0.1μmlongAgNWs,theratioincreasedfrom1.18to
126.89astheAgNWconcentrationincreasedfrom0.005to
0.4wt%.Theconductivityreachedamaximumof92.9Sm^{-1}with0.2wt%AgNWsconcentration(figure4(j)).Inthecase
ofthecompositewithalongerAgNWlength,theratioincreased from 2.65×10^3 to 1.97×10^5 with the increasein theAgNWlength,duetotheeffectivejoiningofanincreasednumberofnetworkedAgNWsinthecomposites(figure4(k)).
TodisclosehowtheAgNWswerelocallyjoinedtoge-
ther, finite-difference time-domain (FDTD) modeling ofan
individualAgNW and AgNW junction was conducted. The localized surface plasmon (SP) of a free-standing single AgNW (40 nm diameter, 1.5 μm length) occurred at 364nm,
which was far away from the wavelength of thefemtosecond
laser. Therefore, the joining of AgNWs does not rely on the SP of individual AgNWs (figure S8, supportinginformation). Withthe780nmlaserincidenttotheAgNWjunction,the
free electrons on the metal surface oscillated collectively, leadingtoalocalelectromagneticfieldenhancementinthe

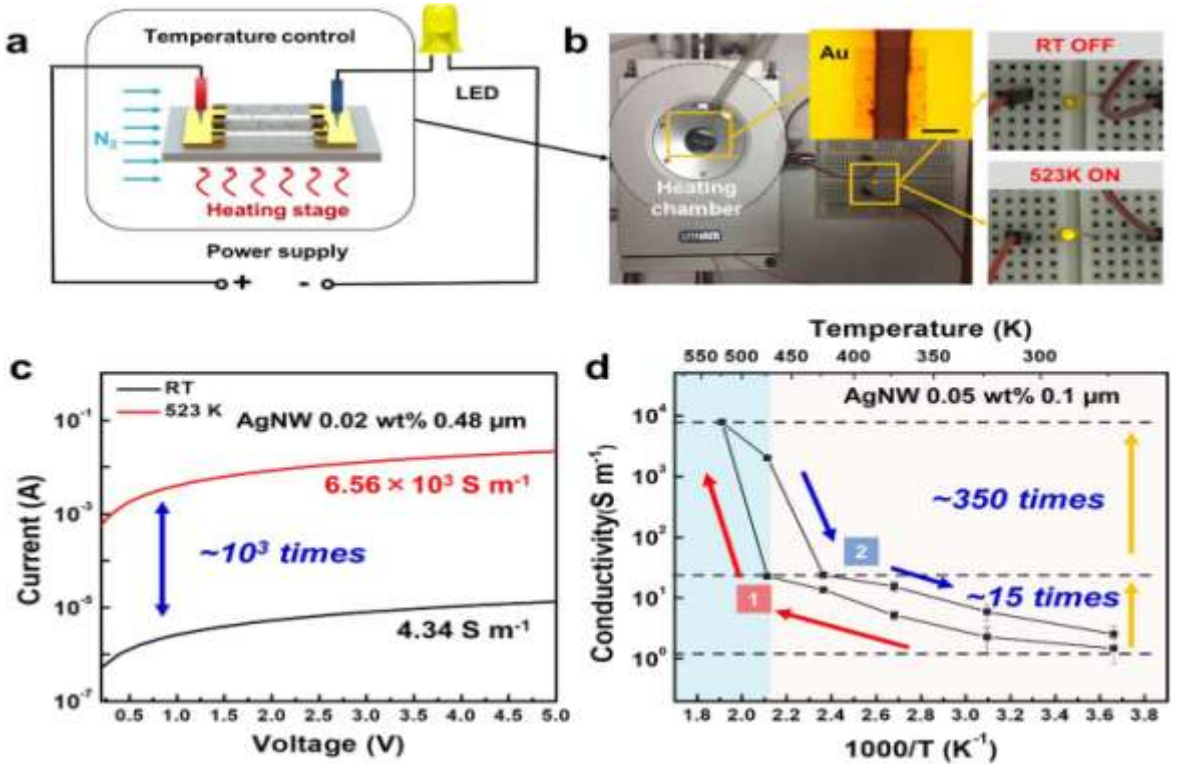

Figure 5.(a) Demonstration of temperature-dependent electrical conductivity of the ATA composites as electrical conductor in an LED circuit. The composite sample was placed in a temperature controllable chamber. (b) Photograph of the ATA composite turning on an LED light when a DC current passes at 523 K. The inset shows the optical image of the bridge bar array. (c) I–V curves of an as-fabricated

bar-shaped channel and thermally treated at 523 K. The AgNW concentration and length were 0.02 wt% and 0.48 μm, respectively.
(d) Temperature-dependent electrical conductivity of the composite with a 0.1 μmAgNW length and a 0.05 wt% AgNW concentration. Red arrows and (1) show the heating process. Blue arrows and (2) show the cooling process. Scale bar: (b) inset: 50 μm.
near field. At the AgNW junction, resonance coupling of SP endowed an intense and durative near-field enhancement of approximately 35 times the incident light, which suggests the occurrenceofthelocalizedjoiningeffectsofthenanowires,
matchedwithourexperimentalresults(figures4(g)and(h),
figure S8, supporting information).
Therefore, both experimental and numerical simulation results confirmed that femtosecond laser irradiation provided a direct, efficient, and selective nanojoining of AgNWjunc- tions in ATA composite, resulting in significantly improved electrical performance.

Temperature-dependent electrical conductivity ofATAcomposite
Torevealthephysicaloriginoftheelectricalchargetransport in the composites and explore the potential device applica- tions, temperature-dependent studies of the ATA composites were conducted. As a proof-of-principle demonstration for electronic devices, an array of bar-shaped channels
($5 \times 5 \times 100$ μm^3W × H × L) fabricated between two Au electrodes usingthe ATA composite (0.02wt% AgNW concentration, 0.48 μm long-AgNWs) were connected in a simple circuit with a light-emitting diode (LED) (figure5(a)).
The sample was placed in a heating chamber with nitrogen gasprotectiontocontrolthetemperature.Whenthetemper-
ature increased from room temperature (RT) to 523 K, the LEDwaslitwithaDCvoltageof10V(figure5(b)).The LEDwentoffasthetemperaturedecreasedbacktoRT.The compositeconductivityincreasedfrom4.34Sm^{-1}atRTto $6.56\times10^4$$Sm^{-1}$at523K(figure5(c)).Thisresultisaclear
demonstration of thetemperature-dependent conductive ATA
composites and their potential for temperature-dependent electronic devices.
Temperature-dependent I–V curves were collectedfor
composites with different AgNW lengths and a fixed con- centration of 0.05 wt%. The temperature was controlled below 523 K to avoid spheroidization of the AgNWsand
decomposition of the polymer matrix. Figure 5(d) depictsthe
two-stage conductivity increase of the ATA composite with
0.1 μm long AgNWs. The conductivity first increased slowly by ∼15 times from 273 to 473 K and then increased abruptly by ∼350 times from 473 to 523 K. Thistemperature

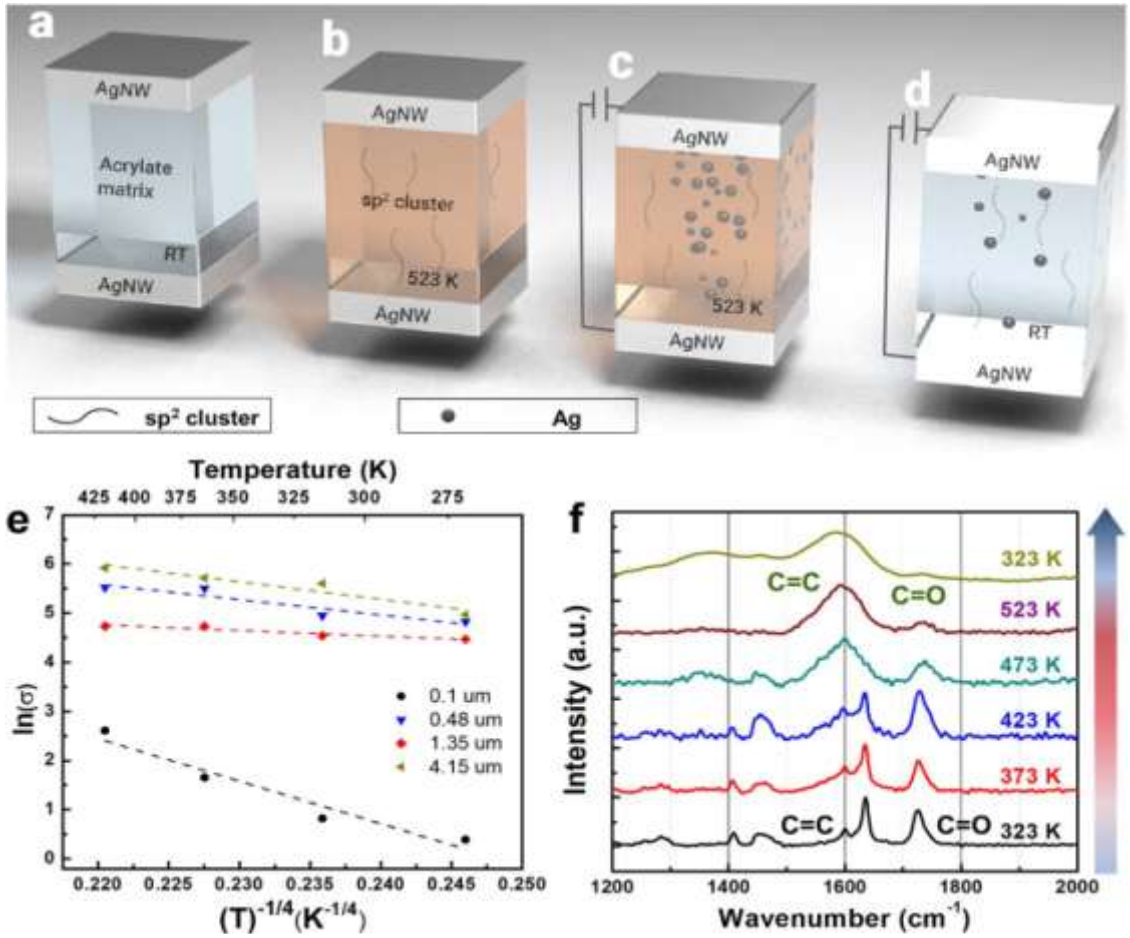

Figure 6.Schematic concept of the resistive switching mechanisms for the ATA composites. (a) Junction structure, (b) formation of sp^2 clusters of acrylate polymer by thermal treatment, (c) temperature- and field-induced Ag filament formation, and (d) recovery to high resistanceatRT.(e)Theconductivity(ln(σ))dataofthecompositesdescribedbytheVRHmodelfora3Dtransportmechanism.TheAgNW lengthwaskeptat0.05wt%.Alldatawerelinearlyfitted.(f)Temperature-dependentRamanspectraoftheATAcompositesrangedfrom298
to 523 K. The AgNW length and concentration were 0.48 μm and 0.05 wt%, respectively. The average laser power used for Raman spectroscopy was 10 mW (wavelength 514.5 nm).

dependency of electrical conductivity was reversible and applicable for all composite samples. In Stage 1, from 273 to 473K,chargecarrierswereactivatedbyelevatedtemperature with a stable increase in conductivity, showing the semi- conducting behavior of the composites [35]. Using the slopes ofanArrheniusplot,theactivationenergy$E_A$wasdetermined
for quantitative analysis (figure S10(b), table S2, supporting information).InStage2,from473to523K,thecomposite
exhibited a jump in electrical conductivity and reached a maximumof$3.6\times10^5 Sm^{-1}$at523K(0.05wt%AgNWconcentration,0.48μmAgNWlength).Thisjumpincon-
ductance was demonstrated to be a typical resistiveswitching phenomenon [36] and occurred by the combination of temperature and field-assistedexcitation.

Reversibleswitchingmechanismofelectricalconductance

The I–V measurement revealed that the temperature-depen- dent reversible switch of electrical conductance was repro- ducible in the ATA composites. This two-stage variation of electrical conductivity can be described by the VRHmodel
[37] in Stage 1 (from 273 to 473 K) and reversible switching model in Stage 2 (from 473 to 523K). The reversible
switching was attributed to carbonaceous pathways that resulted from degradation of the organic polymer [38]
(figures 6(a) and (b)) and metallic Ag filament formation across the polymer matrix (figures 6(c) and (d)).

In order to clarify the electrical conductance enhance- ment by the AgNW loading in Stage 1, a 3D Mott's variable hopping model, which is a model depicting the low

temperature conduction in strongly disordered systems with localized states, was used to calculate the variation of elec- trical conductivity with elevated temperature [39]:

$$\sigma(T)=\sigma^{0}\exp\left[-\left(\frac{T_0}{T}\right)^{1/4}\right] \quad (1)$$

where σ^0 is the temperature-independent prefactor, which represents the limiting value of the conductivity at infinite temperature; and T_0 is the characteristic temperature, which is inversely proportional to the localization length of the charge carriers, thus a small T_0 implies a weak localization and increased conductivity [40]. In figure 6(e), $\ln(\sigma)$ versus $T^{-1/4}$ for the composite resins is plotted and fitted for the ATA composites with different AgNW lengths. The characteristic temperature T_0 and linear quality factor R^2 for each sample are summarized in table S2 (supporting information). The characteristic temperature T_0 decreased from 1.44×10^9 K (pure acrylate) to 1.85×10^4 K (ATA composite, 1.35 μm long AgNWs), indicating a reduced localization of the charge carriers and thus enhanced electrical conductivity [41]. In addition, a diminishing tendency of T_0 and R^2 as the AgNW length increased was observed. Since the metallic ohmic conductance and VRH conductance had the opposite temp- erature dependences [42], the decreased values of T_0 and R^2 implied that the number of metallic ohmic contacts in the composites increased as the length of the AgNWs got longer, which is consistent with the fact that laser nanojoining is more effective on composite resins with long AgNW lengths. However, in the case of the ATA composite with 4.15 μm long AgNWs, the values of T_0 slightly dropped due to the formation of large clusters that enlarged the hopping distance in the composite.

In Stage 2, the internal chemical reactions and structural phase transitions of the composites were studied by temper- ature-dependent Raman spectroscopy [43] (figure 6(f)). In the authors' composite system, the glassy transition temperature (T_g) for acrylate monomer was found to be 286 K [44], which was unlikely to be the cause of the reversible switching at around 473 K. As shown in the Raman spectra, the transition occurred in a temperature range from 423 to 523 K, that resulted in three Raman peaks at ~1366, ~1593, and 1731 cm^{-1}, which were ascribed to the D, G, and C=O bands. As the temperature increased, the G band intensity slowly increased from RT to 473 K and then increased abruptly until 523 K. The significantly increased sp^2 bonding indicated the degradation of the acrylate matrix, which was promoted with the AgNWs serving as the catalyst [45], creating specials sp^2 cluster pathways with high electron mobility within the polymer medium (figure 6(b)). However, the G band intensity did not drop as the temperature decreased, indicating a permanent degradation of the polymer matrix.

At temperatures above 473 K, resistive switching behavior occurred with a threshold voltage of 10 V, ascribed to electro- migration-induced Ag filament formation (figures S11(a)–(c), supporting information). When an electric field was applied, due to the increased Ag mobility at high temperatures, Ag atoms dissociated from individual AgNWs to form bridging filaments among the closest AgNWs, bringing them together to form electrical contacts (supported by the nanoparticle forma- tion around AgNW junctions, figure S11(d), supporting infor- mation). This Ag filament formation was demonstrated in a single AgNW junction [46] and AgNWs/polystyrene compo- sites [47]. Furthermore, when the bias was removed, the fila- ments were ruptured, which can be attributed to the thermal motion of Ag atoms within the filaments. Finally, at tempera- tures below 473 K, the Ag mobility was limited; and the AgNWs were kinetically trapped, returning the ATA composite back to a high-resistance state (figure 6(d)).

The authors' findings demonstrated that the resistive switching of ATA composites can be explained by a combi- nation of sp^2 carbon cluster pathways and Ag filaments. It is promising that micro/nanostructures made of the ATA com- posite material can be engineered to exhibit prominent temp- erature- and electrical-field-dependent electrical behaviors.

III. CONCLUSIONS

In this work, a new strategy was presented for realizing metallic 3D micro/nanostructures with ATA composites via TPPfollowedbyafemtosecondlasernanojoiningprocess.By employing thiol functionalization, TPP-compatible ATA composite resins were obtained with AgNWs uniformly dis- persed in a polymer matrix. Micro/nanoscale 3Dconductive structures were successfully fabricated with ~200 nm reso- lution.Moreover,afemtosecondlaserirradiationprocesswas conductedtofurtherenhancetheelectricalconductivityofthe solidified ATA composites by up to 10^5 times, resulting from the effective joining of AgNW junctions. A strong temper- ature dependence of the conductivity of the ATA composite was observed and analyzed, revealing the charge carriers' transport mechanism following the VRH and reversible switching models. The nanomaterial assembly and joining method demonstrated in this study represent a new opportu- nity for developing functional devices for a broad range of applications, such as 3D electronics, temperature sensors, memristors, MEMS/NEMS, and biomedicaldevices.

Experimental section

Materials

PentagonalAgNWs:0.1mmoll^{-1}monodispersedpentagonal- shaped AgNWs with a diameter of 40 nm and lengths varying from 0.1 to 0.3 μm in isopropyl alcohol (IPA) solutions were purchased from SciventionsInc. (supporting information, figure S1).LongAgNWs:20mgml^{-1}AgNWsdispersedinIPA solutionswere purchased from ACS Material, LLC. The AgNWshad an average diameter of 40 nm and average lengths of >30 μm(figure S1, supporting information). Acrylate pho- toresist: di-trimethylolpropanetetraacrylate (Di-TMPTTA), ben- zyl-2-(dimethylamino)-4′-morpholinobutyrophenone (BDMP), and 6-Mercapto-1-hexanol (6-MCH) were purchased from Sigma Aldrich.

Photoresistpreparation

Homemade ATA composite resins were prepared by direct mixing ofthiol-functionalized AgNWs, acrylic monomer (Di-TMPTTA), and photoinitiator (BDMP). First, theAgNW aqueous solutions underwent ultrasonic agitation(agitation power: 60 W, SONIFIER®SLPe Energy and Branson Ultra- sonics)from30,60,to120mintoreducetheaveragelength to 4.15, 1.35, and 0.48 μm, respectively. The surface mod- ification of AgNWs was then performed by mixing theliquid thiol 6-MCH with the aqueous AgNW solution at a con- centrationof10mmoll^{-1}.Theaqueoussolutionunderwenta120minultrasonicbath,resultingintheformationofthiol-cappedAgNWs. Excess IPA solvent was removed from the solution obtained using high-speed centrifugation (10 min at 15000 rpm, bench top centrifuge Z230M, HermleLabor- technik GmbH). After the centrifugation, the IPA was eva- porated completely from the precipitation. The remnantthiol- capped AgNWs were dispersed in acrylic monomer with concentrations varying from 0.005, 0.02, 0.05, 0.2,to 0.4 wt%.Photoinitiator was added to the dispersion with a constant concentration of 1 wt% in all samples. The compo- siteresinsunderwentultrasonicagitationfor60sfollowedby a magnetic stirring for 24 h at RT (VWR, standard hot plate stirrer). They were then purified using centrifugation (30 min at6000rpm,minispin5452,Eppendorf)toremovelarge AgNW aggregations from the resins. The as-prepared resins werestoredinbrownglassbottlesandstirredcontinuously.

Two-photonpolymerization

TPP fabrication was performed on a 3D laser lithography system (Nanoscribe GmbH, Photonic Professional). A fre- quency-doubled, Er-fiber laser (center wavelength of 780nm, pulse width of 100 fs, repetition rate of 80 MHz, and max- imum power of 150 mW) was used as the irradiation source. An oil immersion objective lens (63 ×and 1.4 NA) was used to focus the laser beam.

Femtosecond lasernanojoining

A femtosecond Ti:sapphire laser with a regenerative ampli- fication system (center wavelength of 800 nm, pulse

width of 120fs,repetitionrateof1KHz)wasemployedinthelaser nanojoining experiment. The laser beam was linearly polarizedwithaGaussianenergydistribution(Msquaredfactor <1.2).Ahalf-waveplateandapolarizerwereusedtoadjust the laser pulse energy. A plano-convex lens with a focal length of 100 mm was used to focus the laser beam. The sample was stationed on an X–Y–Z stage, and the stage was vertically displaced 4 mm from the focal plane to have a defocused beam of 170 μm spot size on the sample surface. Thelaserbeamscannedthesamplesurfacebymovingthe samplestageataspeedof100μms^{-1}.

Scanning electronmicroscopy

A field-emission SEM (Hitachi, S4700) with an acceleration voltage of 5–10 kV was used for the observation andanalysis of the TPP-fabricated structures and AgNW morphology. A chromium layer of 5 nm thick was deposited on the samples beforetheSEMcharacterizationtopreventtheelectriccharge effect.

Tunneling electronmicroscopy

A HRTEM (FEI Tecnai Osiris) with a voltage of 200 kV was used for analyzing the AgNW distribution and femtosecond laser nanojoining. Pristine AgNW TEM samples were pre- pared by drop casting on copper grids with Formvar/carbon supporting film and 400 mesh. The AgNW-acryliccomposite TEMsampleswerepreparedbydirectTPPwritingofasingle layerthinfilmonthesamekindofcoppergrid.

Laser ablation ambient massspectrometry

The laser ablation ambient mass spectrometry system consists of three major modules: a KrFexcimer laser (COMPexPro205 F, wavelength = 248 nm, pulse duration = 23 ns, Coherent Inc.), a time-of-flight mass spectrometer (TOF-MS, JEOL, AccuTOF™, JEOL, USA Inc.), and a sample stage. The laser fluence was fixedat8.75Jcm^{-2}.Thelaserbeamwasfocusedatnormal incidence on the samples with a spot sizeof 0.80 × 1.60 mm^2. The voltages of the outer and inner orifices of the TOF-MS were fixedat30and5V,respectively.Thetemperatureoftheskimmer cone was fixed at 100 °C. The accumulation time was 1 s for eachmeasurement.

Temperature-dependent electricalconductivity measurement

To characterize electrical conductivity, bar-shaped channels were fabricated between two Au electrodes with sputtering depositedonthedesiredregionsthroughshadowmasks(Kurt J Lesker, 99.99% purity Au target). The homemadeelectrical conductivity measurement system consisted of a semi- conductor parameter analyzer (Agilent 4155 C), a heating chamber (Linkam Scientific Instruments (UK), 77-800 K, THMS600), a heating power/temperature controller, and a probe station (Cascade Microtech, MPS 150). A liquid nitrogen tank was used for providing a nitrogenenvironment. Beforemeasurements,compositedeviceswereloadedintothe chamber and placed at the center of the heating stage. A purging process was then performed to ensure all of the air waspurgedout.Afterthat,theheatingstagebegantoramp up thetemperaturefrom273to523Katarateof10Kmin^{-1}andthencooleddownatthesamerate.Acurrent–voltage(I–V) sweep was then performed at an incremental temperature of 50K.

Temperature-dependentRamanmicrospectroscopy

Raman microspectroscopy was conducted using a Raman microscope (Renishaw, InVia™ H 18415). To conduct temperature-dependent Raman characterization, thesamples were placed in the same heating chamber (Linkam Scientific Instruments(UK),77-800K,THMS600)usedforelectrical conductivitymeasurements.Theexcitationlaserbeam,witha wavelengthof514.5nm,wasfocusedontothesamplesurface through the chamber window by an objective lens (50×, NA0.75).Beforeeachmeasurement,thepurgingprocesswas performed.Theheatingstagerampedupthetemperaturefrom 273to523Katarateof10Kmin^{-1}.Theaveragelaserpowerusedtoproduce Ramanspectrawas10mW.Ramanspectra were recorded with an accumulation time of 10 s each at an incremental temperature of 50 K.

Opticalcharacterization

The optical absorption was measured using an ultraviolet- visible spectrophotometer (Evolution 201, Thermo Scientific™). The samples were prepared by spin coating (1 min at 1500 rpm, WS-650MZ-23NPPb, Laurell) witha
thickness of 13.5µm.

REFERENCES

[1] Skylar-Scott M A, Gunasekaran S and Lewis J A 2016 Proc. Natl Acad. Sci. 1136137–42 Huang W, Yu X, Froeter P, Xu R, Ferreira P and Li X 2012 Nano Lett. 12 6283 Xu S, Yan Z, Jang K-I, Huang W, Fu H, Kim J, Wei Z,Flavin M, McCracken J and Wang R 2015 Science 347 154

[2] GeJ,YaoHB,WangX,YeYD,WangJL,WuZY,LiuJW, Fan F J, Gao H L and Zhang C L 2013 Angew. Chem. 1251698He W and Ye C 2015 J. Mater. Sci. Technol. 31 581

[3] ChingNN,WongH,LiWJ,LeongPHandWenZ2002 Sensors Actuators A 97 685

[4] Gansel J K, Thiel M, Rill M S, Decker M, Bade K, Saile V, von Freymann G, Linden S and Wegener M 2009 Science3251513

[5] SoukoulisCMandWegenerM2011Nat.Photon.5523

[6] Chen X, Sun K, Zhang E and Zhang N 2013 RSC Adv. 3 432QiaoZ,YangX,YangS,ZhangLandCaoB2016Chem. Commun.52 7998

[7] André J C 2017 From Additive Manufacturing to 3D/4D Printing 2: Current Techniques, Improvements andTheir Limitations (New York: Wiley) p 121

[8] SpangenbergA,HobeikaN,StehlinF,PierreMalvalJ, Wieder F, Prabhakaran P, Baldeck P and Sopper O 2013Updates in Advanced Lithography (Rijeka: InTech)

[9] FarahaniRD,DubéMandTherriaultD2016Adv.Mater. 28 5794

[10] Radke A, Gissibl T, Klotzbücher T, Braun P V and Giessen H 2011 Adv. Mater. 233018 Huang T Y, Sakar M S, Mao A, Petruska A J, Qiu F, Chen X B, Kennedy S, Mooney D and Nelson B J 2015 Adv. Mater.27 6644

[11] XuBB,XiaH,NiuLG,ZhangYL,SunK,ChenQD,XuY, LvZQ,LiZHandMisawaH2010Small61762Wang H, Liu S, Zhang Y-L, Wang J-N, Wang L, Xia H, Chen Q-D, Ding H and Sun H-B 2015 Sci. Technol. Adv. Mater. 16 024805Blasco E, Müller J, Müller P, Trouillet V, Schön M, Scherer T, Barner-Kowollik C and Wegener M 2016 Adv. Mater. 283592Hu Q, Sun X-Z, Parmenter C D, Fay M W, Smith E F, RanceGA,HeY,ZhangF,LiuYandIrvineD2017Sci.Rep. 7 17150

[12] BakhtinaNA,LoeffelmannU,MacKinnonNandKorvinkJG 2015 Adv. Funct. Mater. 251683Xiong W, Liu Y, Jiang L J, Zhou Y S, Li D W, Jiang L, SilvainJFandLuYF2016Adv.Mater.282002Ushiba S, Shoji S, Masui K, Kono J and Kawata S 2014 Adv.Mater.26 5653

[13] Tabrizi S, Cao Y, Lin H and Jia B 2017 Sci. China Phys., Mech. Astron. 60034201 Masui K, Shoji S, Asaba K, Rodgers T C, Jin F, Duan X-M and Kawata S 2011 Opt. Express 19 22786

[14] HuN,FukunagaH,AtobeS,LiuYandLiJ2011Sensors11 10691

[15] MurphyCJandJanaNR2002Adv.Mater.1480

[16] PengP,LiuL,GerlichAP,HuAandZhouYN2013Part. Part. Syst. Charact. 30 420

[17] JiangX,ZengQandYuA2007Langmuir232218

[18] TanH,ZhanTandFanWY2006J.Phys.Chem.B11021690 JiangL,XiongW,ZhouY,LiuY,HuangX,LiD, Baldacchini T, Jiang L and Lu Y 2016 Opt. Express 2413687

[19] Sokołowski K, Szynkowska M I, Pawlaczyk A, Łukomska-Szymańska M and Sokołowski J 2014 ActaBiochim. Pol. 61317–23

[20] Brostow W, Gorman B P and Olea-Mejia O 2007 Mater.Lett.61 1333

[21] Jonušauskas L, Lau M, Gruber P, Gökce B, Barcikowski S, Malinauskas M and Ovsianikov A 2016 Nanotechnology 27154001

[22] Xiong W, Zhou Y S, He X N, Gao Y, Mahjouri-Samani M, Jiang L, Baldacchini T and Lu Y F 2012 Light: Sci. Appl. 1e6

[23] Rekštytė S, Jonavičius T, Gailevičius D, Malinauskas M, MizeikisV,GamalyEGandJuodkazisS2016Adv.Opt. Mater.4 1209

[24] GuneyMandFedderG2016J.Micromech.Microeng.26105011.